

## Physicochemical studies on some selected oxaloyldihydrazones and their novel palladium(II) complexes along with using oxaloyldihydrazones as corrosion resistant

Ayman H. Ahmed, A.M. Hassan, Hosni A. Gumaa, Bassem H. Mohamed & Ahmed M. Eraky

To cite this article: Ayman H. Ahmed, A.M. Hassan, Hosni A. Gumaa, Bassem H. Mohamed & Ahmed M. Eraky (2017): Physicochemical studies on some selected oxaloyldihydrazones and their novel palladium(II) complexes along with using oxaloyldihydrazones as corrosion resistant, *Inorganic and Nano-Metal Chemistry*, DOI: [10.1080/24701556.2017.1357595](https://doi.org/10.1080/24701556.2017.1357595)

To link to this article: <http://dx.doi.org/10.1080/24701556.2017.1357595>

 View supplementary material 

 Accepted author version posted online: 31 Jul 2017.

 Submit your article to this journal 

 View related articles 

 View Crossmark data 



**Physicochemical studies on some selected oxaloyldihydrazones and their novel palladium(II) complexes along with using oxaloyldihydrazones as corrosion resistants**

**Ayman H. Ahmed<sup>1,2\*</sup>, A.M. Hassan<sup>1</sup>, Hosni A. Gumaa<sup>1</sup>, Bassem H. Mohamed<sup>1</sup>, Ahmed M. Eraky<sup>1</sup>**

<sup>1</sup>*Department of Chemistry, Faculty of science, Al-Azhar University, Nasr City, Cairo, Egypt.*

<sup>2</sup>Chemistry Department, College of Science and Arts, Al Jouf University, Algrayuat, Saudi Arabia.

E-mail: \*Author to whom correspondence should be addressed; e-mail address: ayman\_haf532@yahoo.com

Tel: +2022629357

Fax: +2022629358

**Abstract**

New palladium (II) oxaloyldihydrazone complexes are reported and characterized. The mode of bonding as well as the structure of the isolated compounds have been ascertained on the basis of data obtained from elemental analyses (CHNM), spectral (UV-Vis., IR, mass and <sup>1</sup>H NMR) and thermal (TG and DTA) measurements. Some optical parameters such as indirect optical band

gap and refractive index were estimated for the isolated compounds. The inhibitive properties of all synthesized hydrazones toward the corrosion of carbon-steel in 1 M HCl solutions were tested. The adsorption of hydrazone inhibitors on steel surface proceeded as a spontaneous first order reaction.

**Keyword:** Hydrazone complexes; Spectral investigation; Optical properties; Inhibition.

## 1. Introduction

Actually, the synthesis of hydrazones and their derivatives may lose much as they have wide applications in biology [1], medicine [2], catalysis [3], corrosion inhibition [4] and analytical chemistry [5]. In fact, little papers have been reported for oxaloyldihydrazones or their complexes due to their poor solubility in most organic solvents. Oxaloyldihydrazones are only soluble in much more polar solvents such as DMF and DMSO which means much intensive effort is required to separate such compounds or their complexes in pure crystalline form. Nevertheless some transition metal complexes of oxaloyldihydrazones have been studied [6,7], palladium complexes of the selected oxaloyldihydrazones have not been actually isolated yet. Nowadays, some hydrazone complexes have been accommodated in zeolite-Y by alternative methods and inferred by various physicochemical characterization techniques [8].

Organic inhibitors usually protect the metal or alloy by forming an interstitial hydrophobic film on the metal surface. In general, organic compounds containing polar groups including nitrogen, sulfur, and oxygen have been reported to be good corrosion inhibitors [9]. In fact many Schiff bases including hydrazones are found to be effective corrosion inhibitors of metals [10,11].

The present work was carried out to study the coordination behavior of Pd<sup>II</sup> ions toward the selected oxaloyldihydrazones. Furthermore, the work aims to growing up numbers of semiconductors. For this purpose, the energy gap of used ligands and their relevant complexes have been determined to describe their electronic behaviors. The study was extended to

investigate the inhibition efficiency of all ligands toward carbon-steel in hydrochloric acid solution and some thermodynamic parameters have been calculated.

## 2. Experimental

### 2.1. Chemicals and Equipments

The aldehydes were obtained from Merck Company. Palladium (II) acetate, diethyl oxalate, hydrazine monohydrate were purchased from Sigma-Aldrich. Oxalaldehyde dihydrazide was prepared by reacting diethyl oxalate (1 mol) with hydrazine hydrate (2 mol) [12], (Exp/Lit. m.p = 240/240 °C). Other chemicals and solvents were of highest purity and used without further purification. The  $^1\text{H}$  NMR spectra were recorded on a Jeol-FX-90Q Fourier NMR spectrometer at 25 °C using DMSO solvent and TMS as an internal standard. Mass spectra of the ligands were performed by a Shimadzu-GC-MS-QP1000 EX using the direct inlet system. Metal contents (% wt) were estimated complexometrically by EDTA using xylenol orange (indicator) and solid hexamine buffer (pH = 6). Elemental analyses (CHN), spectral (UV-Vis. and FT-IR) and thermal (TG and DTA) measurements were executed as mentioned elsewhere [13]. The optical band gap energy ( $E_g$ ) of product compounds was calculated from Tauc's equations [14,15]. Corrosion test was performed on freshly prepared Carbon-steel (C-steel) sheet of the chemical compositions (wt %) depicted in Table 1. Prior to the experiment, the specimens were polished with emery papers (220-800 grades) until the surface appears free from any scratches and other apparent defects, then washed with distilled

water followed by degreasing in absolute ethanol and acetone, dried at room temperature, weighed and finally stored in a moisture free desiccators prior to use [16].

## 2.2. Preparations

### 2.2.1. Preparation of oxaloyldihydrazone ligands

In view of the importance of oxaloyldihydrazones and their chelates, we have undertaken the synthesis of four ligand structures including bis(salicylaldehyde)oxaloyldihydrazone ( $L_1$ ), bis(2-hydroxy-1-naphthaldehyde)oxaloyldihydrazone ( $L_2$ ), bis(2-hydroxyacetophenone)oxaloyldihydrazone ( $L_3$ ), bis(2-methoxybenzaldehyde)oxaloyldihydrazone ( $L_4$ ). Oxalicydihydrazide (0.01 mol) dissolved first in hot water (20 cm<sup>3</sup>) followed by adding methanol (40 cm<sup>3</sup>) was mixed with the appropriate aldehydes [salicylaldehyde, 2-hydroxy-1-naphthaldehyde, 2-hydroxyacetophenone and 2-methoxybenzaldehyde] (0.02 mol) in absolute methanol. The resulting mixture went on refluxing for 3 hrs under constant stirring. The product was separated out on concentrating the solution to half of its volume and cooling. The crystals of the desired ligand was collected by filtration through a Buchner funnel and dried in an electric oven at 50 °C for 2 h. Afterwards the ligand was recrystallized from DMF-MeOH<sub>aq</sub> mixed solvent, collected, washed thoroughly on filter paper by acetone to remove any excess of DMF and then dried in an electric oven at 50 °C for 2 h. The molecular structure of the resulting hydrazones was elucidated by elemental analyses and spectral (IR, mass and <sup>1</sup>H NMR) measurements (Table 2,3).

### 2.2.2. Preparation of solid complexes

The dihydrazone ligand (1 mmol) was dissolved in 20 ml DMF (20 ml) and then 50 ml methanol was added. The resulting solution was added slowly to a methanolic solution of palladium(II) chloride. The metal salt was dissolved first in a minimum amount of distilled water (20 ml) before making the methanolic solution. Worthy mention, the Pd(II) chloride was mixed first with NaCl in 1:2 ratio to give a soluble solution. The resulting mixture was heated under reflux for 3-4 hrs and then reduced to 15 cm<sup>3</sup> by gentle heating on hot plate. The resulting reaction mixture was cooled down to room temperature and the colored solid complexes were filtered off, washed several times with successive portions of hot solvents (DMF, methanol and acetone, respectively) to remove any excess of unreacted ligands. Finally, the desired products were dried in an electric furnace at 80 °C for 6 hrs.

### 2.3. Dihydrazone ligands as corrosion inhibitors

#### 2.3.1. Solutions

The aggressive solutions, 1 M HCl, were prepared by dilution of analytical grade HCl with distilled water. Stock solutions of the inhibitors were prepared in DMF. All test solutions contained 10 ml (20 vol.%) of DMF to ensure solubility. The concentrations of the used inhibitors (L<sub>1</sub>-L<sub>4</sub>) were 5×10<sup>-4</sup>, 1 × 10<sup>-4</sup>, 5 × 10<sup>-5</sup> and 1×10<sup>-5</sup> M.

#### 2.3.2 Gravimetric measurements

A simple test for measuring corrosion is the gravimetric method (weight loss). The method involves exposing a clean weighed piece of the alloy to the corrosive environment for a specified time followed by cleaning to remove corrosion products and weighing the piece to determine the loss of weight.

A previously weighed alloy (C-steel) was completely immersed in 50 ml of the test solution (1M HCl) in an open beaker. The beaker was maintained at a temperature of 301 K. The coupons were suspended in the beakers with the aid of glass hooks. In the absence of inhibitors, the coupons were retrieved from their corrosive solutions at 1 h interval for 3 hrs. Further measurements were carried out after introduction of the additives (L<sub>1</sub>-L<sub>4</sub>) at concentrations  $5 \times 10^{-4}$ ,  $1 \times 10^{-4}$ ,  $5 \times 10^{-5}$  and  $1 \times 10^{-5}$  M in the beaker maintained at the room temperature for the same duration. The coupons were withdrawn from the test solution at 1 h interval progressively for 4 hrs, dipped into saturated ammonium acetate solution at room temperature to terminate the corrosion reaction, washed by scrubbing with a light brush, rinsed in acetone and finally dried in an oven at 80 °C before reweighing. The difference in weight in grams was taken as the total weight loss (W) [17].

$$W = W_i - W_f$$

Where:  $W_i$  and  $W_f$  are the initial and final weights for aluminum, respectively.

Each reading reported is an average of three experimental reading recorded to the nearest 0.0001 g on an Adam184 electronic weighing balance. The value of corrosion rate,  $\rho$  (in  $\text{gm.cm}^{-2}.\text{min}^{-1}$ ) was calculated from the following equation [17]:

$$\rho = \frac{W}{A \times t}$$

Where: W = weight loss to the nearest 0.0001gm, A = area of specimen to the nearest  $0.01 \text{ cm}^2$  ( $2 \times$  area of one surface/face) and t = exposure time (minutes).

The inhibition efficiency ( $\% \eta$ ) for each inhibitor and the degree of surface coverage ( $\theta$ ) were calculated using the equations [17]:

$$\eta\% = \left[ 1 - \frac{\rho_1}{\rho_2} \right] \times 100\%$$

$$\theta = 1 - \frac{\rho_1}{\rho_2}$$

Where  $\rho_1$  and  $\rho_2$  are the corrosion rates in the presence and absence of inhibitor, respectively.

### 2.3.2. Kinetic treatment of weight loss results

The corrosion reaction is a heterogeneous one, composed of anodic and cathodic reactions with the same or different rate [18]. In the present study, the initial weight of steel coupon at time, t is designated  $W_i$ , the weight loss is  $\Delta W$  and the weight change at time, t is  $(W_i - \Delta W)$  or  $W_f$ . When  $\log W_f$  was plotted against time, a linear variation was observed [19]:

$$\log W_f = \log W_i - Kt$$

Where:  $W_i$  = the initial weight before immersion,  $K$  = slope (the rate constant), and  $t$  is time.

Regarding the adsorption reaction on steel surface proceeds as first order, the half-life values,  $t_{1/2}$ , of the metal in the test solutions were calculated from the rate constant values using the equation [19]:

$$t_{1/2} = \frac{\ln 2}{K} = \frac{0.693}{K}$$

### 3. Results and discussion

The entire oxaloyldihydrazones ( $L_1$ - $L_4$ ) and their solid complexes with Pd(II) have been isolated in pure form. Tables 2, 3 declare the analytical, physical and spectroscopic data of the hydrazones and their isolated palladium complexes. The prepared complexes are non-hygroscopic, soluble in strong polar solvents such as in DMF and DMSO but insoluble in MeOH/EtOH, Et<sub>2</sub>O, CHCl<sub>3</sub>, acetone, CCl<sub>4</sub> as well as benzene. The calculated and found element percentages (CHNM%) point out that the compositions of the chelates harmonize with the proposed formulae. Compositions of the solid complexes have been identified on the basis of spectral UV-Vis., IR and NMR. The solvent content in the complexes was determined by thermal (TG and DTA) measurements and the results can be taken as evidence for the suggested structural formulae.

### 3.1. IR Spectra

The comparative IR spectral study of the parent ligands and their palladium(II) complexes demonstrates

the coordination mode of the ligands during the complex formation. The important frequencies with their possible assignments are listed in Table 1 (S1).

Prepared oxloyldihydrazones can be represented either in the trans- (staggered) or cis- (anti-cis- or syn-cis-) configuration as revealing in Fig.1, [20]. The structures of the ligands were authenticated on the basis: (1) The strong bands observed at 1602-1617  $\text{cm}^{-1}$  are assignable to the azomethine group ( $\nu\text{C}=\text{N}$ ). The observation of these bands provides a direct evidence for the interaction of dihydrazides with selected aldehydes. (2) The bands centered at (3149, 3204 and 1666,  $L_1$ ), (3476, 3166 and 1705(m) +1660(v.s),  $L_2$ ) and (3448, 3293 and 1689(m) +1651(v.s),  $L_3$ )  $\text{cm}^{-1}$  are attributed to  $\nu(\text{OH})_{\text{phenolic/naphthoic}}$ ,  $\nu(\text{NH})$  and  $\nu(\text{C}=\text{O})$ , respectively. Meanwhile,  $L_4$  which does not contain ortho-OH group revealed  $\nu(\text{NH})$  at 3202  $\text{cm}^{-1}$  and  $\nu(\text{C}=\text{O})$  at 1653  $\text{cm}^{-1}$ . (3) Both  $\nu(\text{C}=\text{O})$  and  $\nu(\text{NH})$  were appeared concurrently in the IR spectra of all ligands giving a significant reflection to the existence of keto forms. (4) Appearance of  $\nu(\text{C}=\text{O})$  as two bands for each  $L_2$  and  $L_3$  ( $\approx 1700, 1660 \text{ cm}^{-1}$ ) and one band for  $L_1$  and  $L_4$  ( $\approx 1660 \text{ cm}^{-1}$ ) refers to the mixture of [cis(syn/anti-cis-structure) + trans(staggered)-structure] isomers for  $L_2, L_3$  and trans (staggered) structure for  $L_1, L_4$ , respectively, (Fig. 1). This suggestion can be pictured by the so called field effect criteria where the cis isomer is absorbed at higher frequency than trans one [12]. The band observed at 1705 and 1689  $\text{cm}^{-1}$  characterized trans form while the other two bands located at 1660 and 1653  $\text{cm}^{-1}$  indicated the presence of cis-form. (5) Foundation of OH (phenolic) group in  $L_1$  as sharp at lower position (3149  $\text{cm}^{-1}$ ) evidenced the persistence of

intramolecular H-bonding between the phenolic-OH and CH=N group, (O–H $\cdots$ N), and in the same time ruled out the formation of intermolecular H-bonding between the associated ligand molecules (O–H $\cdots$ O–H) [21]. On the other hand, the existence of two bands at 3278 cm<sup>-1</sup> (L<sub>1</sub>) and 3227 cm<sup>-1</sup> (L<sub>4</sub>) may be attributed to  $\nu(\text{OH})_{\text{enolic}}$  in H-bond bonding with azomethine group. (6) The bands concerning the  $\nu(\text{C}=\text{O})$  in the spectra of L<sub>1</sub> – L<sub>4</sub> were located at 1275, 1287, 1246 and 964 cm<sup>-1</sup>, respectively [21,22]. (7) Also, each ligand contains 3-4 bands in the regions 1400-1600 and 700-800 cm<sup>-1</sup> assignable to  $\nu(\text{C}=\text{C})$  and  $\delta(\text{CH})_{\text{out of plane}}$  of the aromatic ring, respectively.

In case of complexes I-III, obscurity of both  $\nu(\text{NH})$ ,  $\nu(\text{OH})_{\text{phenolic/naphthoic}}$  and  $\nu(\text{C}=\text{O})$  after chelation with splitting of  $\nu(\text{C}=\text{N})$  and positive shift of  $\nu(\text{C}=\text{O})_{\text{phenolic/naphthoic}}$  evidenced that C=O and NH groups did not contribute in coordination whereas the corresponding ligand binds to the palladium in dienol form via the azomethine and deprotonated o-hydroxyl groups [23]. The splitting of C=N was occurred due to the enolization of two C=O groups in dihydrazone molecule assuming dienol skeleton. The appearance of  $\nu(\text{OH})_{\text{enolic}}$  in I and III at lower frequencies, (3238 and 3194 cm<sup>-1</sup>, respectively) are due to the formation of H-bond between two generated enolic (OH) groups [24]. However, the obscure of  $\nu(\text{OH})_{\text{enolic}}$  in II accompanied with the foundation of  $\nu(\text{M}-\text{O}_{\text{enolic}})$  is most probably due to the deprotonation of enolized carbonyl (C–OH) upon coordination with the palladium ion. The existence of new bands attributed to  $\nu(\text{M}-\text{O}_{\text{phenolic}})$  boosts the formation of complexes I-III [25, 26]. In the case of IV, positive shift of  $\nu(\text{C}=\text{O})$  in addition to the observation of  $\nu(\text{NH})$  and  $\nu(\text{C}=\text{N})$  at nearly the same locations excluded the involvement of these groups in coordination and referred to persistence of L<sub>4</sub> ligand in diketo form. The lower positive shift of  $\nu(\text{C}-\text{O})_{\text{methoxy}}$  upon chelation indicates the weak

interaction between Pd<sup>II</sup> ion and ortho-methoxy (-OMe) group. On the other hand, crystalline and coordinated water molecules in all palladium complexes (I-IV) were presumed based on the appearance of the broad bands within the range 3300-3500 cm<sup>-1</sup>, Table 3, [27]. By the way, the slight changes in the positions of  $\nu(\text{C}=\text{C})_{\text{ph}}$  for all free ligands upon chelation arise from the metal-ligand interaction.

### 3.2. <sup>1</sup>H NMR Spectra

The main signals of <sup>1</sup>H NMR spectra of the ligands and some Pd(II) complexes are summarized in Table 2.

Virtually, NMR spectroscopy is considered a powerful technique employed to identify the skeleton of the ligands. <sup>1</sup>H NMR spectra of all ligands exhibited multiple signals of the aromatic protons in the 6.5–8.5 ppm region. The signals of equal integration observed in L<sub>1</sub>, L<sub>2</sub> and L<sub>3</sub> at  $\delta$  (12.6, 11), (12.8, 12.6) and (12.9, 11.8) ppm downfield of TMS have been assigned to NH and ortho-OH protons, respectively. On the other hand, L<sub>4</sub> revealed a signal at 12.3 ppm attributed to secondary NH group. Upon the addition of D<sub>2</sub>O then OH and NH signals were obscured. Further, the existence of the  $\delta\text{OH}$  (phenolic/naphthoic) at its normal frequency excluded any intramolecular hydrogen bonding operating between ortho-OH and CH=N group (CH=N.....H-O). The azomethine signals,  $\delta(\text{CH}=\text{N})$ , observed only in L<sub>1</sub>, L<sub>2</sub> and L<sub>4</sub> have been assigned at 8.75, 9.73 and 8.95 ppm, respectively. As reported in the literature [24,28], if the dihydrazone exists in the syn-cis-configuration or staggered configuration, the  $\delta\text{OH}$ ,  $\delta\text{NH}$  and  $\delta\text{CH}=\text{N}$ , resonances, each should appear as a singlet. However, the appearance of these signals in the form

of six signals (doublet of doublet) indicates anti-cis (chair) configuration. Actually, the features of the  $^1\text{H-NMR}$  spectra of the dihydrazones are in conformity with syn-cis- or staggered configuration. According to IR interpretation mentioned above, the staggered configuration is well defined/dominated for all ligands ( $\text{L}_1\text{-L}_4$ ).  $^1\text{H NMR}$  spectra of  $\text{L}_3$  and  $\text{L}_4$  differ from other ligands spectra where they showed signals at 2.55 and 3.9 ppm downfield of TMS due the methyl ( $\text{CH}_3$ ) and methoxy ( $\text{OCH}_3$ ) protons, respectively [1,9].

The assignments of the main signals in  $^1\text{H NMR}$  spectra of some diamagnetic palladium complexes II, III and IV in comparison to that of free ligands ( $\text{L}_2$ ,  $\text{L}_3$  and  $\text{L}_4$ ) are given in Table 2 (S2). The data demonstrated the following facts. For II and III complexes: no signal is detected for a naphthoic/phenolic OH or secondary NH groups. This remark gives a clue for the deprotonation of both ortho- OH groups upon complexation. Obscurity of secondary NH in the same complexes ruled out its contribution in coordination where its proton migrated to the carbonyl oxygen ( $\text{C=O}$ ) forming an enolized carbonyl ( $\text{C-OH}$ ). Appearance of  $\nu(\text{M-O}_{\text{enolic}})$  in the IR spectrum of complex II emphasized the deprotonation of the enolized carbonyl by complexation. Participation of azomethine nitrogen atoms in coordination with the metal centre is conspicuous in the shift of  $\delta(-\text{CH=N})$  associated with complex II to higher frequency by 0.246 ppm. In case of sample IV: four signals are observed in the region 12.80 -10.90 ppm and 12.80 - 10.90 ppm assuming doublet doublet of both secondary NH and  $\text{CH=N}$  protons, respectively [29]. This result proves the existence of  $\text{L}_4$  ligand in chair conformation [39] with a cis-configuration of dihydrazone. The upfield shift observed for  $\delta(-\text{OCH}_3)$  by 0.58 ppm upon complexation inferred the involvement of this group in bonding without removal of  $\text{CH}_3$  group.

The signals concerned to the aromatic protons of all Pd(II) complexes were observed within 6 - 8.4 ppm with minor changes in their positions compared with free hydrazones.

### 3.3. Electronic spectra and magnetic studies

The assignments of the observed electronic absorption bands of the oxaloylhydrazones as well as their metal complexes in DMF are shown in Table 3 [26,30,31]. The electronic data of the investigated ligands exhibited five peaks at 350-392 (n- $\pi^*$ , C=N), 338-375 (n- $\pi^*$ , C=O), 306-340 ( $\pi$ - $\pi^*$ , C=N), 292-315 ( $\pi$ - $\pi^*$ , C=O), and 280-303 ( $\pi$ - $\pi^*$ , aromatic ring) nm. It was noticed that the essential features of the spectrum of the complexes were entirely different when compared with that of the free ligand, which boosted the coordination of used ligands with the palladium ions. The spectra of all Pd<sup>II</sup> complexes in DMF, Table 3, revealed three broad peaks at 475-510, 390-470 and 340- 430 nm assigned to ( $^1A_{1g} \rightarrow ^3A_{2g}$ ,  $^3B_{1g}$ ), ( $^1A_{1g} \rightarrow ^1A_{2g}$ ) and 390 ( $^1A_{1g} \rightarrow ^1B_g$ ) transitions, respectively. Additionally, complex III exhibited an additional band at 370 nm attributed to ( $^1A_{1g} \rightarrow ^1E_g$ ) transition. This suggests a square-planar environment around the Pd<sup>II</sup> ion. Pd(II) complexes are diamagnetic as expected.

### 3.4. Thermal studies

To examine the thermal stabilities of Pd<sup>II</sup>-complexes, thermogravimetric analysis (TG) and differential thermal analysis (DTA) for all complexes were done (Fig. 2). For complex I, TG

curve showed four stages of decomposition at 45, 250, 320 and 800 °C. The first stage corresponds to the loss of 0.5 crystalline water (found/calculated % = 0.5/1.5) and accompanied by endothermic peak in DT curve. The other three decomposition stages refer to the initial decomposition temperature of the complex with formation of an expected Pd and/or PdO residue at the last stage. In DTA curve, the exothermic peak observed at mid point 300 °C reflects the decomposition while the endothermic peak at mid point 789.9 °C which is not accompanied by weight loss is most probably attributed to a phase change. This endothermic effect arises from the crystal structure change of some products resulted from the complex degradation. TG data of complex II, exhibited three stages of decomposition at 50-100, 250-420 and 550-870 °C. The first stage which is accompanied by endothermic effects in DTA curve corresponds to expelling of two crystalline water (found/calculated% = 5.1/5.1) while the other two stages concerned to the gradual decomposition of the complex with formation of (Pd + PdO) mixture (found/calculated%= 32.4/32.2) at the last stage. The exothermic peak observed at mid point equals 330 °C (DTA curve) refers to the decomposition of the solid complex. The TG curve of complex III showed five stages of decomposition at 40-150, 200-280, 280-425, 425-570 and 570-720 °C, The first stage corresponds to the loss of 2.5 crystalline water molecules (found/calculated% = 9.0/8.9) while the other four stages corresponds to the gradual decomposition of the complex with formation of a mixture of Pd and PdO at the last stage (found/calculated% = 44.9/45.2). DTA curve exhibited an endothermic peak at 60 °C corresponding to loss of crystalline water molecules meanwhile the remarkable exothermic peak at 261.99 pointing to the decomposition of the complex. TG and DT thermograms of complex IV revealed four steps of decomposition where the first step is related to the elimination of two

crystalline water molecules from the complex formula (found/calculated% = 5.2/6.1) while the other three steps observed in the regions 250-320, 350-450, 650-900 °C are relevant to the gradual decomposition with formation of PdO and/or Pd residue at the last stage as occurred with other analogous complexes (I-III).

On the basis of the various physico-chemical and spectral studies presented above and their discussion, the complexes may be suggested to have structures shown in Fig. 3 (palladium complexes were drawn by ChemDraw Ultra 8.0 program).

### 3.5. Optical properties

The optical and the electrical properties of metals complexes are interesting due to great potential application in Schottky diode, solid state devices and optical sensor [32]. To clarify the conductivity of the isolated complexes, the optical band gap ( $E_g$ ) of oxaloyldihydrazone ligands and their Pd(II) complexes have been calculated with the help of absorption spectra. To calculate the optical band gap energy from absorption spectra, Tauc's relation is used [13,14]:

$$\alpha h\nu = A(h\nu - E_g)^m$$

Where  $h\nu$  is the photon energy,  $h$  is Planck's constant,  $\alpha$  is the absorption coefficient,  $E_g$  is the optical energy gap,  $A$  is the constant,  $m$  is equal to 1/2 and 2 for direct and indirect transitions, respectively.

The absorption coefficient ( $\alpha$ ) was calculated from to the relation:

$$\alpha = \frac{1}{d \ln(1/T)}$$

Where  $d$  is the width of the cell and  $T$  is the measured transmittance.

We plot a graph between  $(\alpha h\nu)^2$  versus  $h\nu$ , the extrapolation of the straight line to  $(\alpha h\nu)^2 = 0$  axis gives optical band gap. Figure 4 shows Tauc's plot for all the samples. Band gap for ligands and Pd<sup>II</sup>-complexes in DMF solvent lies in the ranges 3.06-3.42 eV and 2.38-3.39 eV, respectively (Table 2). Careful inspection of data mentioned in Table 2 revealed that the optical band gap values of all ligands ( $E_g$ ) were minimized upon complexation. As reported in the literature [33] it is suggested that after complexation, metal leads to raise mobilization of the ligand electrons by accepting them in its shell. It can be evaluated that after formation of the complex, the chemical structure of the ligands is changed, the width of the localized levels is expanded and in turn, the band gap is smaller. This result is very significant in applications of electronic and optoelectronic devices, because of the lower optical band gap of the materials [34]. Small band gap facilitates electronic transitions between the HOMO-LUMO energy levels and makes the molecule more electro-conductive [35]. Upon excitation, some of the electrons get enough energy to jump the band gap in one go. Once they are in the conduction band, they can conduct electricity, as can the hole they left behind in the valence band. The hole is an empty state that allows electrons in the valence band some degree of freedom. In essence, the obtained band gap values suggest that these complexes are semiconductors and lie in the same range of highly efficient photovoltaic materials. So, the present compounds could be

considered potential materials for harvesting solar radiation in solar cell applications [33,36]. The little difference in the optical band gap  $E_g$  values between all studied complexes may be due to their synonymous chemical structures.

As the refractive index is an important parameter for optical applications, it is important to determine it for ligands and their complexes. The evaluation of refractive indices of optical materials is of considerable importance for application in integrated optic devices such as switches, filters and modulators. Besides, the refractive index is an important physical parameter, which is widely used in chemistry to identify the liquid, or its purity. For this purpose, optical properties were investigated for the compounds by spectrophotometric measurement of transmittance, T, and reflectance, R, at normal incidence in the wavelength range of 190–900 nm. The optical reflectance spectra (R) for oxaloyldihydrazone ligands and their Pd(II) complexes as a function of wavelength ( $\lambda$ ,nm) are shown in Fig. 5. The reflectance has been estimated using the relationship,  $R + T + A=1$ , for normal reflectance, the refractive index value (n) of the compounds may be approximately expressed by the relation [37],

$$n = \frac{(1 + \sqrt{R})}{(1 - \sqrt{R})}, \text{ where } R \text{ is the normal reflectance.}$$

The variations in the refractive index (n) with wavelength ( $\lambda$ ,nm) is presented in Fig. 6. The variation of n values with frequency range indicated that some interactions took place between photons and electrons [38]. Moreover, Fig. 6 clarified that the complexation affects the refractive index of the free ligands where there is a difference in the n values upon connection.

### 3.6. Application

#### 3.6.1. Corrosion inhibition of hydrazones

The inhibitive actions of ligands on the dissolution of C-steel in 1 M HCl are investigated and the inhibition efficiency values of the hydrazone derivatives are depicted in Table 4. Careful inspection of these results showed that, by increasing the inhibitor concentration, both  $(\theta)$  and  $(\eta\%)$  are increased while the weight loss is reduced. So, the dissolution of C-steel in the presence of the investigated inhibitor can be interpreted on the basis of interface inhibition mode where the adsorbed species mechanically screen the coated part of the metal surface from the action of the corrosive medium. This adsorption is related to some discriminated features of the investigated oxaloyldihydrazone like the functional groups (OH, NH, C=O and C=N), quite large molecular size, high molecular weight, aromaticity, electron density at the donor atoms (N:, :O:) and also the  $\pi$ -orbital character of azomethine, carbonyl and phenyl groups. Adsorption and desorption of inhibitor molecules continuously occur at the metal surface and an equilibrium exists between the two processes at a particular temperature. The inhibition achieved by dihydrazone compounds decreases in the sequence  $L_4 > L_3 > L_1 > L_2$  and this behavior can be discussed in what follows. The difference in the inhibition efficiencies of the four compounds lies in their steric factor and electron density at the donor atoms. Nevertheless, all hydrazone ligands are capable to attach to the metal surface, the persistence of methoxy (OMe) group in ( $L_4$ ) which is an efficient electron donating group

than phenolic-OH group present in other compounds facilitates the adsorption on the metal surface. Positive mesomeric effect (+M effect) and negative inductive effect (-I effect) of -OCH<sub>3</sub> leads to increase the electron density over phenyl ring which pushes the electrons towards the donor atoms in O=C-NH-N=CH part by virtue of resonance and subsequently enhances the bond strength between the molecule and the corroding metal [39]. Under these circumstances, the inhibition efficiency of (L<sub>4</sub>) should be higher than other ligands. L<sub>3</sub> came after L<sub>4</sub> as the electron donating nature of the methyl group attached to the azomethine (-N=C(CH<sub>3</sub>)) maximized the electron density on the azomethine group subsequently the ligand to metal surface became more strong. Apparently, L<sub>1</sub> comes before L<sub>2</sub> because the electron pair on the ortho-OH group reaches directly to the azomethine group by delocalization with one phenyl ring while in case of L<sub>2</sub> the naphthyl ring withdraws the electron pair to themselves. Further, existence of two naphthyl rings in the structure of L<sub>2</sub> may cause crowding that encourages incomplete coating. The obtained data, Fig. 7, boosted the application of the utilized ligands especially L<sub>4</sub> as plausible corrosion pickling inhibitors whereas the maximum protection efficiency of L<sub>4</sub> was 47%. It is evident that the inhibition efficiency values are not extremely high owing to the lower ligand concentrations used.

### 3.6.2. Kinetic treatment

Regarding the experimental section, when  $\log W_f$  was plotted against time, Fig. 8, with respect to the abovementioned sheets in HCl solutions, a linear variation was perceived, which confirmed a first-order reaction kinetics [39]. Table 4 gives the rate constants and half life values. It is evident that the rate constants come down with raising the inhibitor concentrations

(L<sub>1</sub>-L<sub>4</sub>) sustaining the inhibition of carbon steel in 1M HCl by the additives. The increase in half life indicates more protection of the metals by the oxaloyldihydrazones [39].

#### 4. Conclusion

In the present study, we have prepared mono and binuclear palladium complexes of dihydrazones and characterized them on the basis of data obtained from physicochemical and spectroscopic studies. The oxaloyldihydrazone ligands (L<sub>1</sub>-L<sub>4</sub>) can be synthesized by usual condensation of oxaloyldihydrazide with salicylaldehyde, 2-hydroxy-1-naphthaldhyde, 2-hydroxyaceto-phenone and 2-methoxy-benzaldehyde, respectively, in a 1:2 molar ratio. The dihydrazone is bonded in I and III as a dibasic tetradentate giving mononuclear complexes while in complex II, the dihydrazone acts as a tetrabasic hexadentate providing binuclear complex. The ligand behaves in dibasic bidentate manner in the remaining complex IV. The obtained complexes may tentatively be suggested to have square planar structures. Indirect band gaps of all samples lie in the range of wide band gap semiconductors. Corrosion test reflects the capability of the investigated ligands to mitigate the corrosion of C-steel in HCl solution especially L<sub>4</sub>.

## References

- [1] El-Wahab, H. A.; El-Fattah, M. A.; Ahmed, A. H.; Elhenawy, A.A.; Alian, N. A. J. *Organomet. Chem.* **2015**, 79, 99-106.
- [2] Alam, M. S.; Choi, S.; Lee, D. *Bioorg. Med. Chem.* **2017**, 25, 389-396.
- [3] Ghorbanloo, M.; Jafari, S.; Bikas, R.; Krawczyk, M. S.; Lis, T. *Inorg. Chim. Acta* **2017**, 455, 15-24.
- [4] Gupta, S. R.; Mourya, P.; Singh, M. M.; Singh, V. P. *J Organomet. Chem.* **2014**, 767, 136-143.
- [5] Bishnoi, S.; Milton, M. D. *Tetrahedron Lett.* **2015**, 56, 6633-6638.
- [6] Ahmed, A. H.; Hassan, A. M.; Gumaa, H. A.; Mohamed, B. H.; Eraky, A. M. *Cogent Chemistry* **2016**, 2, 1-14.
- [7] Koch, A.; Phukan, A.; Chanu, O. B.; Kumar, A.; Lal, R. A. *J. Mol. Struct.* **2014**, 1060, 119-130.
- [8] Ahmed, A. H. *Rev. Inorg. Chem.* **2014**, 34, 153-175 and references therein.
- [9] Finšga, M.; Jackson, J. *Corros. Sci.* **2014**, 86, 17-41.
- [10] Singh, A. K.; Singh, P.; *J. Ind. Eng. Chem.* **2015**, 21, 552-560.

- [11] Singh, D. K.; Kumar, S.; Udayabhanu, G.; John, R. P. *J. Mol. Liq.* **2016**, 216, 738-746.
- [12] Ali, A. M.; Ahmed, A. H.; Gumaa, H. A.; Mohamed, B. H.; Eraky, A. M. *J. Chem. Pharm. Res.* 2015, 7, 91-104 and references therein.
- [13] Salama, T. M.; Ahmed, A. H.; El-Bahy, Z. M. *Micropor. Mesopor. Mater.* **2006**, 89, 251-259.
- [14] Rashad, M. M.; Hassan, A. M.; Nassar, A. M.; Ibrahim, N. M.; Mourtada, A. *Appl. Phys.* **A2013**, 117, 877-890.
- [15] Tauc, J. *Mater. Res. Bull.* **1968**, 3, 37-46.
- [16] NACE, Unofficial NACE Publication 1984, 102.
- [17] Mohammed-Dabo, I. A.; Yaro, S. A.; Abubakar, G.; Ayilara, S. I.; Apugo-Nwosu, T. U.; Akuso, S. A. *J. Basic. Appl. Sci. Res.* **2011**, 1, 1989-1999.
- [18] James, A. O.; Akaranta, O. *African Journal of Pure and Applied Chemistry* **2009**, 3, 262-268.
- [19] Okafor, P. C.; Ebenso, E. E.; Ekpe, U. J. *Int. J. Electrochem. Sci.* **2010**, 5, 978-993.
- [20] Lat, R. A.; Adhikari, S.; Kumar, A. *In. J. Chem.* **1997**, 36, 1063-1067.
- [21] Burger, K.; Ruff, I.; Ruff, F. J. *Inorg. Nucl. Chem.* **1965**, 27, 179-190.
- [22] Chanu, O. B.; Kumar, A.; Ahmed, A.; Lal, R. A. *J. Mol. Struct.* **2012**, 1007, 257-274.

- [23] Salapathy, S.; Sahoo, B. J. *Inorg. Nucl. Chem.* **1970**, 32, 2224-2227.
- [24] Kumar, A; Lal, R. A.; Chanu, O. B.; Borthakur, R.; Koch, A.; Lemtur, A.; Adhikari, S.; Choudhury, S. J. *Coord. Chem.* **2011**, 64, 1729–1742.
- [25] Ferraro, J. R. *Low Frequency Vibration of Inorganic and Coordination Compounds*, Plenum, New York, 1971.
- [26] Ali, A. M; Ahmed, A. H.; Mohamed, T. A.; Mohamed, B.H. *Transit. Met. Chem.* 2007, 32, 461-467.
- [27] , A. M; Ahmed, A. H.; Mohamed, T. A.; Mohamed, B. H. *J. App. Sci. Res.* 2007, 3, 109-118.
- [28] Lal, R. A.; Basumatary, D.; Chakraborty, J.; Bhaumik, S.; Kumar, A. *Ind. J. Chem.* 2006, 45, 619-628.
- [29] Jackman, L. M.; Sternbell, S. *Applications of Nuclear Magnetic Resonance Spectroscopy in Organic Chemistry* pergamon press, oxford, 1978.
- [30] Sutton, D.; *Electronic Spectra of Transition Metal Complexes*, McGraw Hill, London, 1968.
- [31] Lever, A. B. P. *Inorganic Electronic Spectroscopy*, Elsevier Publishing Company, Amsterdam, 1984.
- [32] Tao, X. T.; Suzuki, H.; Watanabe, T.; Lee, S. H.; Miyata, S.; Sasabe, H. *Appl. Phys. Lett.* 1997, 70, 1503-1505.
- [33] Karipcin, F.; Dede, B.; Caglar, Y.; Hur, D.; Ilican, S.; Caglar, M; Sahin, Y. *Opt. Commun.*

2007, 272, 131–137

[34] Turan, N.; Gündüz, B.; Körkoca, H.; Adigüzel, R.; Çolak, N.; Buldurun, K. *J. Mex. Chem. Soc.* 2014, 58, 65-75.

[35] Sengupta, S. K.; Pandey, O. P.; Srivastava, B. K.; Sharma, V. *Transit. Met. Chem.* 1998, 23, 349-353.

[36] Fu, M. L.; Guo, G.C.; Liu, X.; Cai, L. Z.; Huang, J. S. *Inorg. Chem. Commun.* 2005, 8, 18-21.

[37] Gittleman, J. I.; Sichel, E. K.; Arie, Y. *Sol. Energy Mater.* 1979, 1, 93-104.

[38] Yakuphanoglu, F.; Erten, H. *Opt. Appl.* 2005, 4, 969-976.

[39] Margerum, J. D.; Mller, L. J. *Photochromism*, Wiley Interscience, New York, 1971.

**Table captions**

Table 1. Specifications of C-steel coupons used for weight loss measurements.

Specimen	C	Si	As	Sn	Mn	P	S	Cr	Ni	Pb	Zn	Cu	Al	Fe	Mo	Co	Nb	Ti	V	W
C- steel	0.07	0.01	-	-	0.39	0.022	0.0001	0.04	0.04	0.003	-	0.073	0.03	-	0.009	0.016	0.0006	0.003	0.017	.013

Table 2. Analytical, physical and spectroscopic data of the oxaloyldihydrazones and their related metal complexes.

Compound.	Symbol	M.p(°C)	Found(Cald.)%				<sup>1</sup> H-NMR Chemical shift (δppm)	μ <sub>eff.</sub>	M <sup>+</sup> Found/calcd.	E <sub>g</sub> (eV)
		Color	C	H	N	M				
C <sub>16</sub> H <sub>14</sub> N <sub>4</sub> O <sub>4</sub>	L <sub>1</sub>	>300	59.1	5.4	16.2	-	12.6(NH, s), 10.98(OH, s), 8.75(CH=N, s), 6.6-8.40 (aromatic protons, m)	-	326.0/ 326.0	3.10
		Yellow	(58.9)	(4.3)	(17.2)	-				
C <sub>24</sub> H <sub>18</sub> N <sub>4</sub> O <sub>4</sub>	L <sub>2</sub>	>300	68.1	5.3	12.9	-	12.76(NH, s), 12.57(OH, s), 9.74(CH=N, s), 7.0-8.8 (aromatic protons, m)	-	427.1/426.4	3.06
		Yellow	(67.7)	(4.3)	(13.2)	-				
C <sub>18</sub> H <sub>18</sub> N <sub>4</sub> O <sub>4</sub>	L <sub>3</sub>	>300	59.5	6.1	14.7	-	12.85(NH, s), 11.85(OH, s), 6.6-8.0(aromatic protons, m), 2.48(CH <sub>3</sub> , s)	-	356.4/354.2	3.32
		Pale Yellow	(61)	(5.1)	(15.8)	-				
C <sub>18</sub> H <sub>18</sub> N <sub>4</sub> O <sub>4</sub>	L <sub>4</sub>	>300	59.2	5.8	15.7	-	12.3(NH, s), 11.9(OH, s), 8.95(CH=N, s), 6.8-8.5(aromatic protons, m), 3.93(OCH <sub>3</sub> , s)	-	355.0/354.4	3.42
		White	(61)	(5.1)	(15.8)	-				
[Pd(L <sub>1</sub> -2H)].0.5H <sub>2</sub> O	I	>300	44.0	3.7	13.1	23.2	very weak bands	Diamg	-	2.25
		Orange	(43.7)	(3.0)	(12.7)	(24.2)				
[Pd <sub>2</sub> (L <sub>2</sub> -4H)(H <sub>2</sub> O) <sub>2</sub> ].2H <sub>2</sub> O	II	>300	41.4	3.4	8.2	30.2	9.98(CH=N, s), 6.8-8.6 (aromatic protons, m)	Diamg	-	2.55
		Orange Red	(40.7)	(3.1)	(7.9)	(30.1)				
[Pd(L <sub>3</sub> -2H)].2.5H <sub>2</sub> O	III	>300	43.2	4.3	11.2	21.5	6.6-8.2(aromatic protons, m), 2.55(CH <sub>3</sub> , s)	Diamg	-	2.38
		Pale Yellow	(42.9)	(4.2)	(11.1)	(21.1)				
[Pd(L <sub>4</sub> )(Cl) <sub>2</sub> ].2H <sub>2</sub> O	IV	>300	39.1	4.2	10.2	19.7	12.8-10.8(NH, q), 9-8.1(CH=N, s), 6.4-8 (aromatic protons, m), 3.35(OCH <sub>3</sub> , s)	Diamg	-	3.25
		Orange	(38.1)	(3.9)	(9.9)	(18.7)				

Table 3. Significant IR and electronic absorption data of oxaloyldihydrazones and their palladium complexes.

Symbol	$\nu(\text{OH})$ phenolic (enolic)	$\nu(\text{H}_2\text{O})$	$\nu(\text{NH})$	$\nu(\text{C-H})$ aromatic (aliphatic)	$\nu(\text{C=O})$	$\nu(\text{C=N})$	$\nu(\text{C-O})$ phenolic	$\nu(\text{C-OMe})$	$\nu(\text{C=C})$	$\delta(\text{C-H})$ aromatic out of plane (carbonyl/methoxy)	$\nu(\text{M-O})$ phenolic/enolic	$\lambda_{\text{max}}$ , nm (assignments)
L <sub>1</sub>	3149	-	3204	3062	1666	1620	1275	-	1403	756	-/-	390(n- $\pi^*$ , C=N), 350(n- $\pi^*$ ,
	(3278)			(2924)					1458		(-/-)	C=O), 340( $\pi$ - $\pi^*$ , C=N), 303
									1486			( $\pi$ - $\pi^*$ , C=O), 292( $\pi$ - $\pi^*$ , Phenyl)
L <sub>2</sub>	3476	-	3166	3043	1705	1621	1287	-	1465	741	-/-	392(n- $\pi^*$ , C=N), 375(n- $\pi^*$ , C=O),
	(-)			(2926)	1660				1541		(-/-)	330( $\pi$ - $\pi^*$ , C=N), 315( $\pi$ - $\pi^*$ ,
									1574			C=O), 303( $\pi$ - $\pi^*$ , Phenyl)
L <sub>3</sub>	-	-	3293	3048	1689	1607	1246	-	1449	746	-/-	372(n- $\pi^*$ , C=N), 352(n- $\pi^*$ ,
	(3227)			(2923)	1651				1486		(-/-)	C=O), 336( $\pi$ - $\pi^*$ , C=N), 305
									1512			( $\pi$ - $\pi^*$ , C=O), 290( $\pi$ - $\pi^*$ , Phenyl)
L <sub>4</sub>	-	-	3202	3041	1653	1600	-	964	1464	760	-/-	350(n- $\pi^*$ , C=N), 338(n- $\pi^*$ ,
	(3238)			(2940)					1486		(-/-)	C=O), 306( $\pi$ - $\pi^*$ , C=N), 292
									1572			( $\pi$ - $\pi^*$ , C=O),

												280( $\pi - \pi^*$ , Phenyl)
I	-	3473	-	3060	-	1621	1287	-	1410	756	550/-	475( $^1A_{1g} \rightarrow ^3A_{2g}$ , $^3B_{1g}$ )
	(-)			(2925)		1638			1457		(-/-)	390( $^1A_{1g} \rightarrow ^1A_{2g}$ )
									1495			340( $^1A_{1g} \rightarrow ^1B_{1g}$ )
II	-	3442	-	3053	-	1617	1296	-	1452	750	589/552	500( $^1A_{1g} \rightarrow ^3A_{2g}$ , $^3B_{1g}$ )
	(-)			(2924)		1644			1530		(-/-)	450 ( $^1A_{1g} \rightarrow ^1A_{2g}$ ),
									1600			425( $^1A_{1g} \rightarrow ^1B_{1g}$ )
III	-	3442	-	3065	-	1632	1262	-	1433	759	555/-	475( $^1A_{1g} \rightarrow ^3A_{2g}$ , $^3B_{1g}$ )
	(3194)			(2927)		1638			1484		(-/-)	440( $^1A_{1g} \rightarrow ^1A_{2g}$ ) ,390
									1513			( $^1A_{1g} \rightarrow ^1B_{1g}$ ), 370 ( $^1A_{1g} \rightarrow ^1E_{1g}$ )
IV	-	3451	3205	3060	1665	1600	-	967	1466	760	-/-	510( $^1A_{1g} \rightarrow ^3A_{2g}$ , $^3B_{1g}$ )
	(-)			(2923)					1486		(-/559)	470( $^1A_{1g} \rightarrow ^1A_{2g}$ ), 430( $^1A_{1g} \rightarrow ^1B_{1g}$ )
									1527			

Table 4. Corrosion parameters for carbon steel coupons in (1M HCl) solution in presence and absence of different concentrations of hydrazone ligands obtained from weight loss measurement at room temperature after 4 hrs immersion time.

Inhibitor	Conc. (M)	Weight Loss (g)	Rate of corrosion $\text{mg cm}^{-2} \text{h}^{-1}$	$\theta$	Inhibition efficiency $\eta$ %
L <sub>1</sub>	Blank	0.0180	0.0046	-	-
	$5 \times 10^{-4}$	0.0120	0.0031	0.32	32
	$1 \times 10^{-4}$	0.0126	0.0033	0.28	28
	$5 \times 10^{-5}$	0.0131	0.0034	0.27	27
	$1 \times 10^{-5}$	0.0132	0.0034	0.26	26
L <sub>2</sub>	Blank	0.0180	0.0028	-	-
	$5 \times 10^{-4}$	0.0073	0.0019	0.31	31
	$1 \times 10^{-4}$	0.0081	0.0021	0.23	23
	$5 \times 10^{-5}$	0.0089	0.0023	0.17	17
	$1 \times 10^{-5}$	0.0096	0.0025	0.11	11
L <sub>3</sub>	Blank	0.0167	0.0043	-	-
	$5 \times 10^{-4}$	0.0094	0.0025	0.43	43
	$1 \times 10^{-4}$	0.0104	0.0027	0.37	37
	$5 \times 10^{-5}$	0.0110	0.0028	0.34	34
	$1 \times 10^{-5}$	0.0124	0.0032	0.26	26
L <sub>4</sub>	Blank	0.0110	0.0028	-	-
	$5 \times 10^{-4}$	0.0057	0.0015	0.47	47
	$1 \times 10^{-4}$	0.0059	0.0015	0.45	45
	$5 \times 10^{-5}$	0.0064	0.0016	0.42	42
	$1 \times 10^{-5}$	0.0069	0.0018	0.36	36

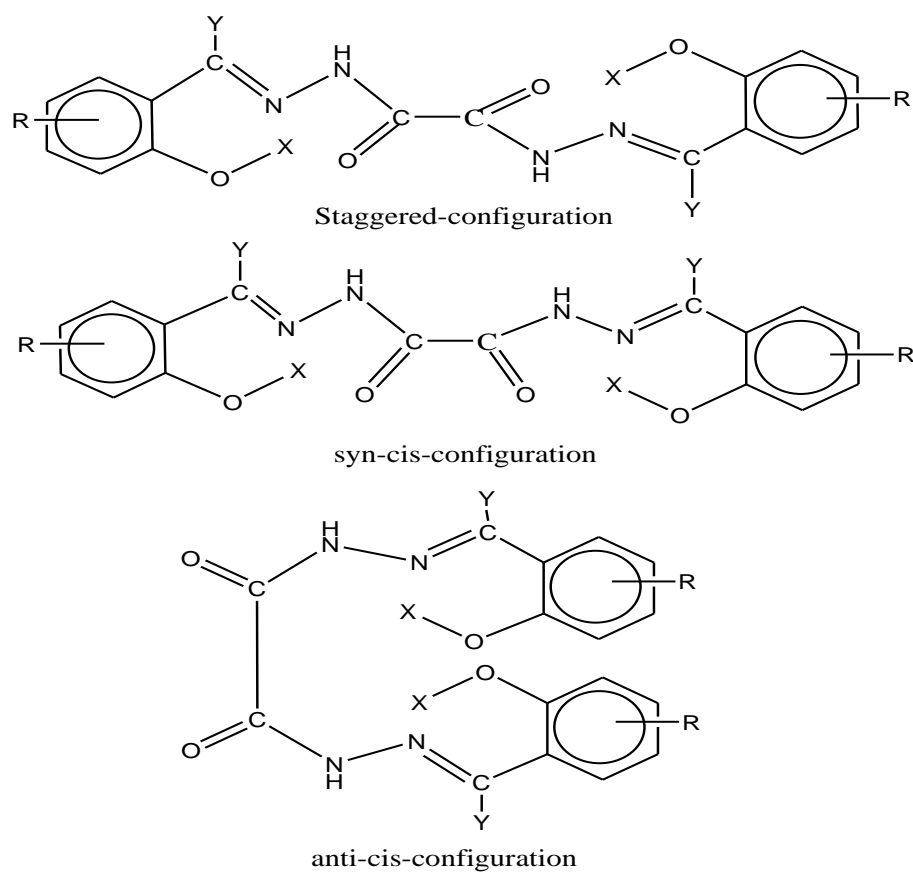


Fig. 1. Proposed structures of oxaloyldihydrazone ligands

Where  $L_1$  ( $R=H$ ,  $X=H$ ,  $Y=H$ ),  $L_2$  ( $R=ph$ ,  $X=H$ ,  $Y=H$ ),  $L_3$  ( $R=H$ ,  $X=H$ ,  $Y=CH_3$ ) and  $L_4$  ( $R=H$ ,  $X=CH_3$ ,  $Y=H$ ).

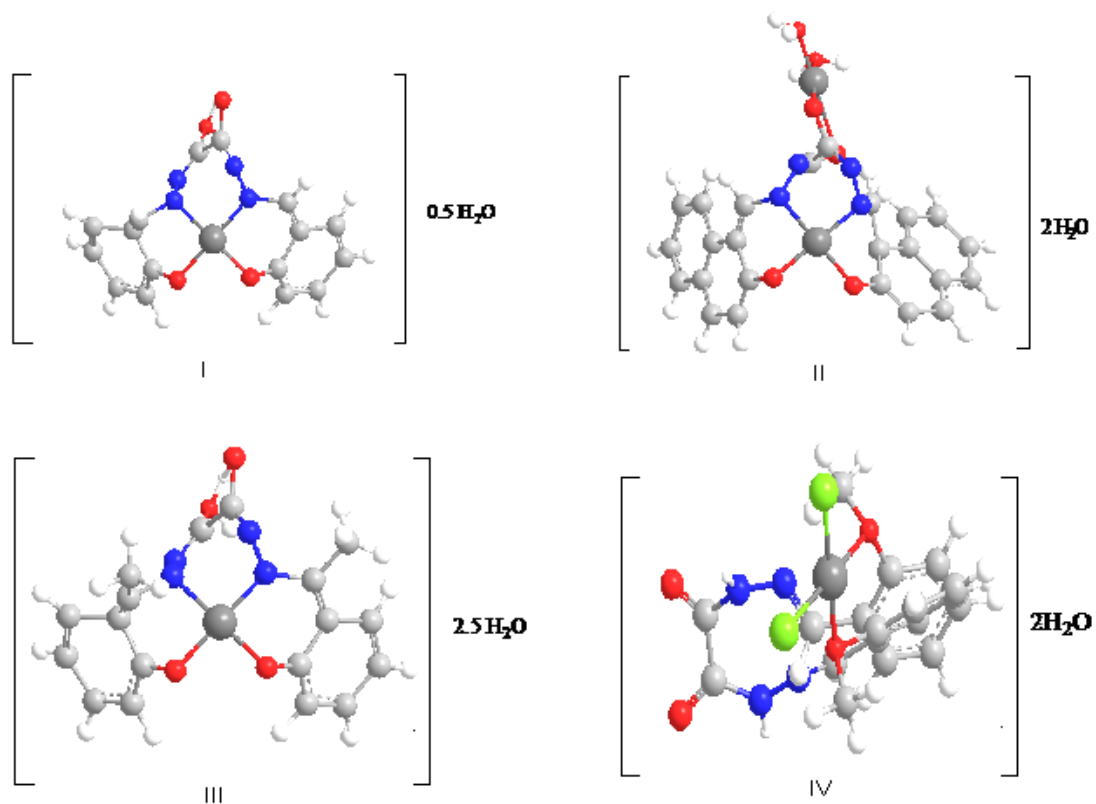


Fig. 2. TGA and DTA curves of Pd(II) complexes (I-IV)

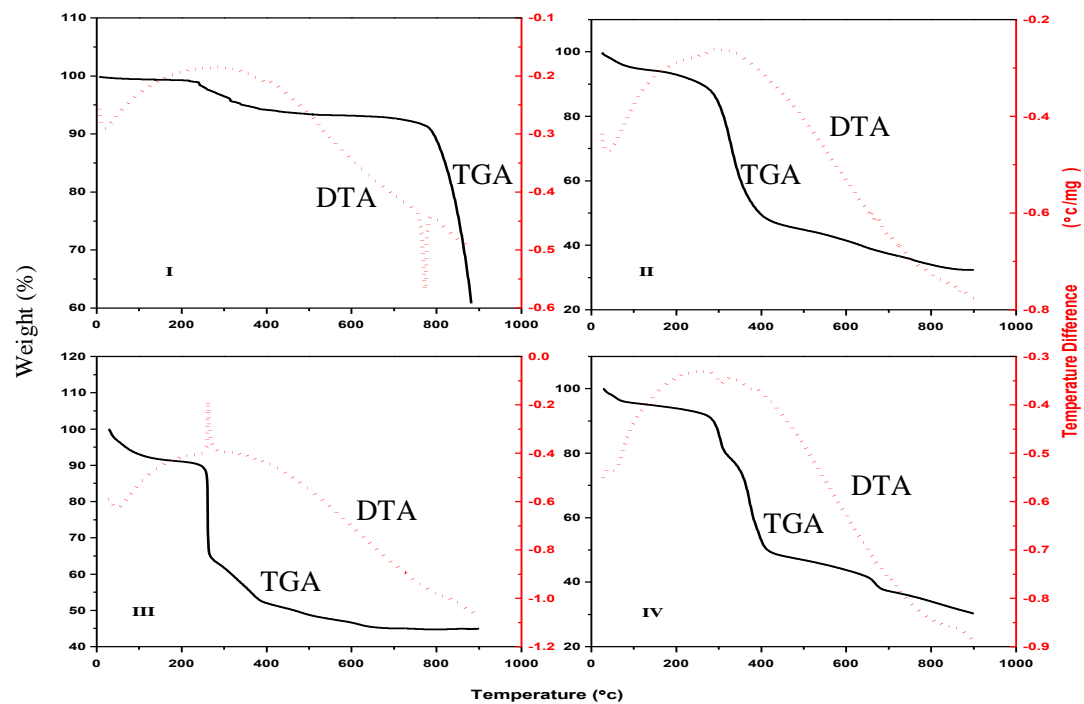


Fig. 3. Suggested 3D structures of Pd<sup>II</sup>-oxaloyldihydrazone complexes.

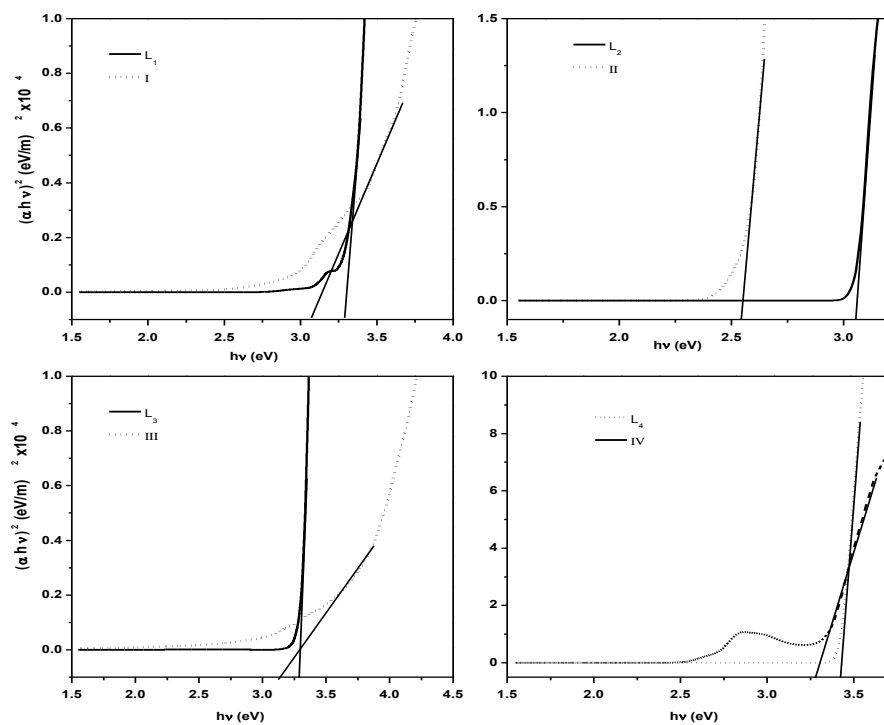


Fig. 4. The plots of  $(\alpha h\nu)^2$  vs.  $h\nu$  of Pd(II) oxaloyldihydrazone complexes.

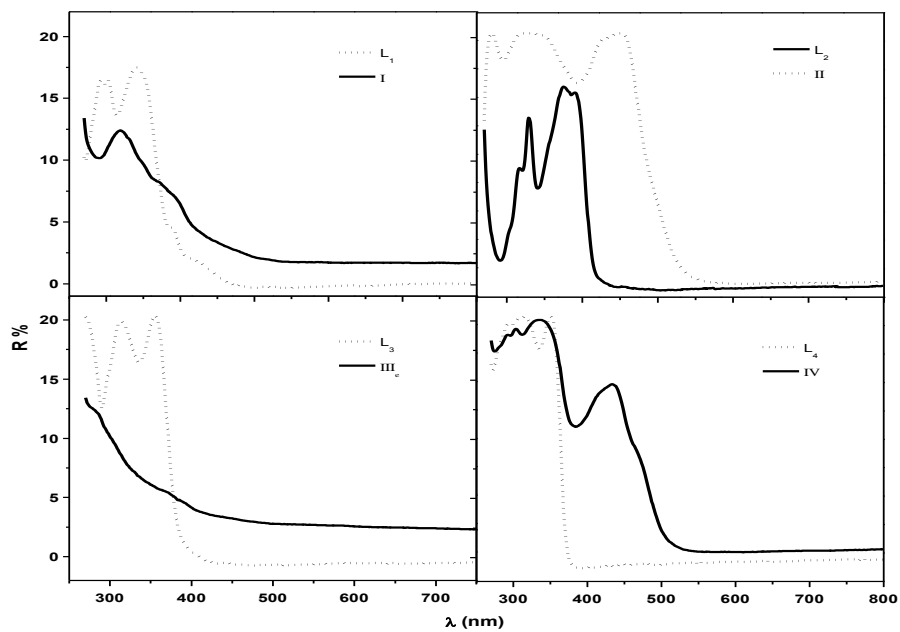


Fig. 5. The optical reflectance spectra (R) for oxaloyldihydrazone ligands and their Pd(II) complexes.

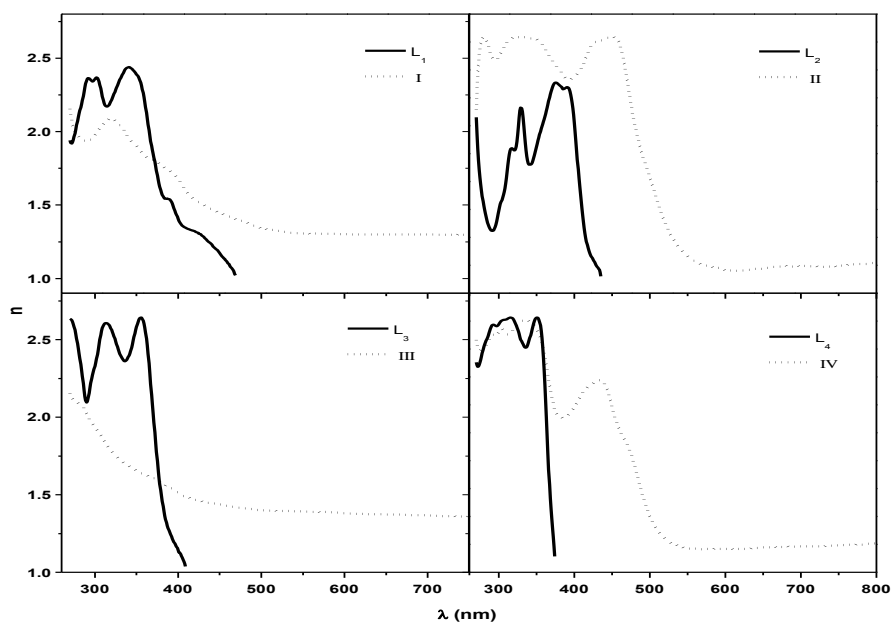


Fig. 6. The variation of the refractive index ( $n$ ) with wavelength ( $\lambda$ ) for oxaloyldihydrazone ligands and their Pd(II) complexes.

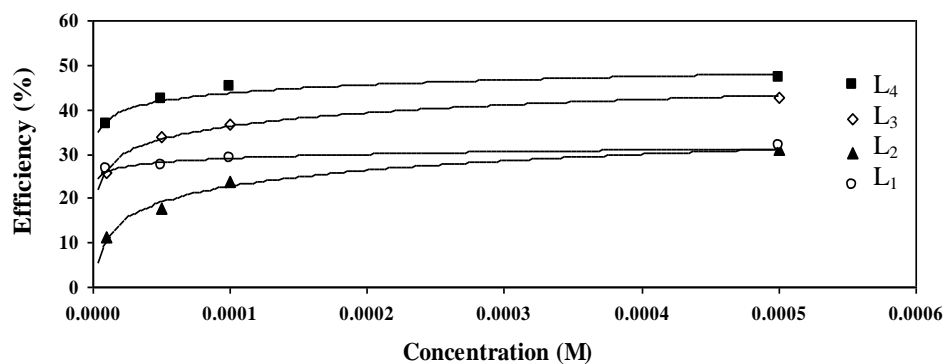


Fig. 7. The efficiency for C-steel sheets in 1M HCl solution in the presence and absence of different concentrations of oxaloyldihydrazone ligands at room temperature.

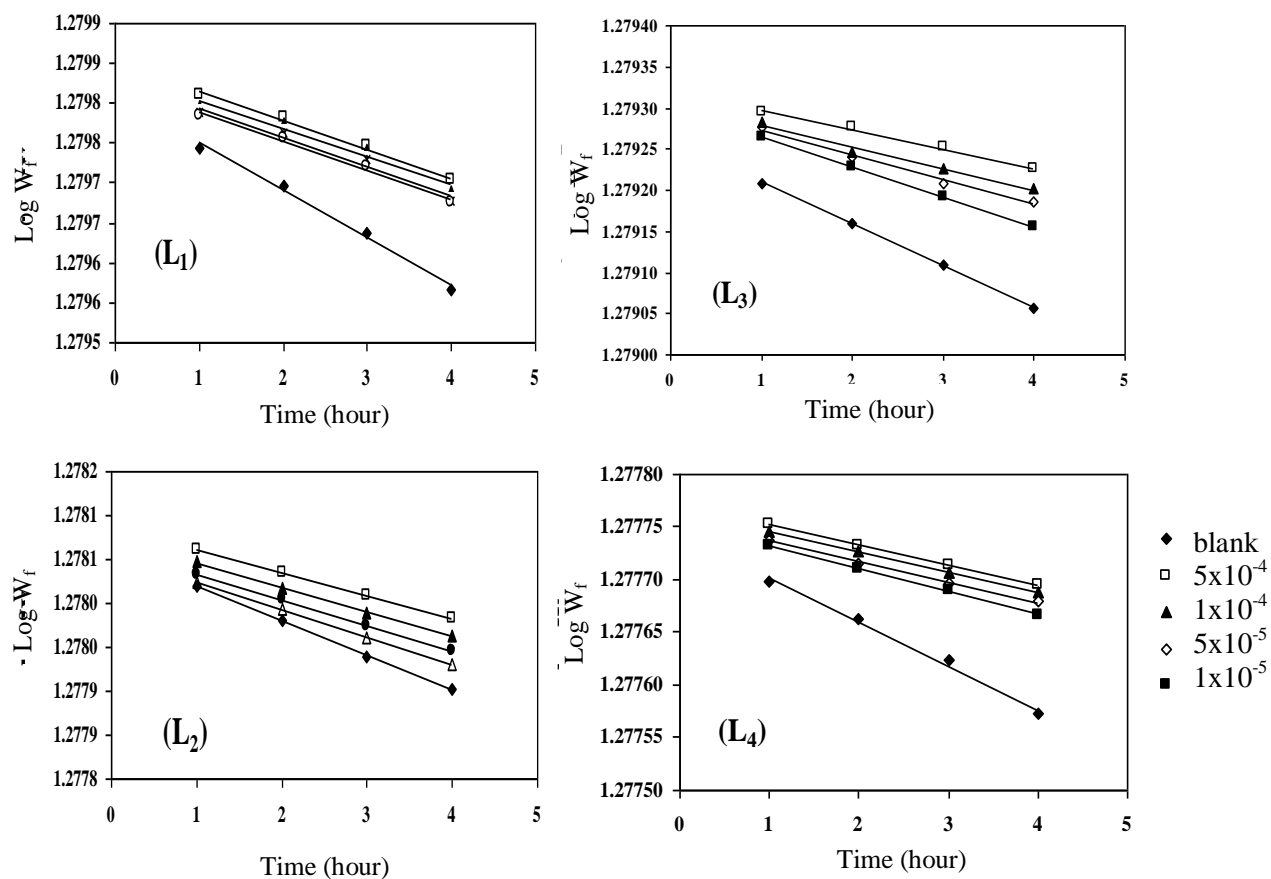


Fig. 8. Variation of  $\log W_f$  with time (hour) for C-steel coupons in HCl solution containing oxaloyldihydrazone ligands (L<sub>1</sub>-L<sub>4</sub>).